New Interpretation of the $\pi N \to \pi N$ Scattering Data and the Charge-Independence Hypothesis

NILS A. TÖRNQVIST
Research Institute for Theoretical Physics, University of Helsinki, Helsinki, Finland
(Received 11 April 1967)

The isospin dependence and the charge independence of the $\pi N \to \pi N$ differential cross sections is studied by a graphical method reported previously. An interesting and not well-known observation is made, namely, that for the non-spin-flip and the spin-flip cross section separately the triangular inequalities are accurately satisfied as equalities at low energies (below 200 MeV), and in backward scattering also at higher energies. This observation, which is believed to be of a fundamental nature, does not have a trivial explanation in the usual formalism. A suggestion is made as to how the formalism could be modified so that the observation would have a simple interpretation as a new kind of unitarity condition.

I. INTRODUCTION

THIS paper is a continuation of a previous one,[1] in which we used a graphical method to study relations and inequalitites following from charge independence (CI). We then applied the method to $\pi N \to \pi N$ total cross sections and were able to describe graphically the well-known isospin effects in the total cross sections.

However, the charge-independence hypothesis applies just as well to differential cross sections. In fact, here the problem is more interesting because of the large number of data available, and because of the possibility that some effect that might exist for differential cross sections may well be "smoothed out" in the total cross sections. It is therefore natural to proceed to analyze the branching ratios, which are obtained from differential cross sections. Our analysis reveals indeed an interesting and not well-known effect, to which we have not been able to find any simple explanation using the usual formalism. This effect is simply that the triangular inequalities reduce to equalities for a large region of energy and momentum transfer.

In the following we first describe briefly the graphical method and its properties (Sec. II). In Sec. III we discuss the results obtained from the analysis of the experimental data. In Sec. IV we define certain linear combinations of the isospin amplitudes which have simple transformation properties under crossing. We then suggest a modification of the isospin formalism which could explain the observations. The new formalism involves a unitarity condition on the S matrix in charge space.

II. THE DIAGRAM

We shall here briefly recapitulate the most important properties of the graphical method.[1,2] The diagram is a barycentric (triangular) coordinate system for three branching ratios. In $\pi N \to \pi N$ there are three charge channels for which the cross sections can easily be measured

$$\pi^+ p \to \pi^+ p, \quad \pi^- p \to \pi^- p, \quad \pi^- p \to \pi^0 n. \tag{1}$$

We define the branching ratios for these as

$$y^{(i)} = \sigma^{(i)}/\sigma, \tag{2}$$

where $\sigma = \sigma^{(+)} + \sigma^{(-)} + \sigma^{(\mathrm{ex})}$ and $i = +, -$, and ex. Then we have trivially

$$y^{(+)} + y^{(-)} + y^{(\mathrm{ex})} = 1, \tag{3}$$

which makes the two-dimensional diagram possible. The triangle inequalities or equivalently the inequality

$$\lambda(\sigma^{(+)}, \sigma^{(-)}, 2\sigma^{(\mathrm{ex})}) \leqslant 0, \tag{4}$$

where

$$\lambda(x,y,z) = x^2 + y^2 + z^2 - 2xy - 2xz - 2yz,$$

which follows from CI, defines an elliptic physical region in the diagram. This is made circular by a special choice of the triangle and by a "scale factor" 1.5 for $y^{(\mathrm{ex})}$. The boundary curve corresponds to the condition $|\cos\varphi| = 1$, where φ is the phase angle between the two isospin amplitudes $A_{1/2}$ and $A_{3/2}$.

Using elementary algebra one can find the following interesting and useful interpretation of the diagram. Namely, if we define the complex number[3]

$$z = \frac{(A_{1/2} + i\sqrt{2}A_{3/2})(A_{1/2} - i\sqrt{2}A_{3/2})^*}{|A_{1/2}|^2 + 2|A_{3/2}|^2}, \tag{5}$$

the diagram can be interpreted simply as the complex z plane, with $z=0$ corresponding to the center of the circle and $|z| = 1$ to the circle itself. The real axis (Rez is proportional to $|A_{1/2}|^2 - 2|A_{3/2}|^2$) passes through the points $N_{1/2}$ and $N_{3/2}$ (see the figures below). The imaginary axis (Imz is proportional to the interference term $\mathrm{Re}A_{1/2}A_{3/2}^*$) is perpendicular to it. The quantity z is useful when one wishes to study the isospin dependence and interpret points in the diagram in terms of the isospin amplitudes.

One further point is of interest. Namely, in any process with a given configuration of intermediate states with definite isospins,[4] the phases of the two isospin

[1] N. Törnqvist, Phys. Rev. 148, 1418 (1966); Nuovo Cimento 43, 255 (1966).
[2] N. Törnqvist, Phys. Rev., this issue, 161, 1581 (1967).
[3] Strictly this expression holds only for differential cross section with definite polarizations. In other cases there should be a summation over spins and integration over momenta both in the numerator and the denominator in (5).
[4] This can be visualized by a Feynman diagram in which all lines have definite isospin. See Ref. 2.

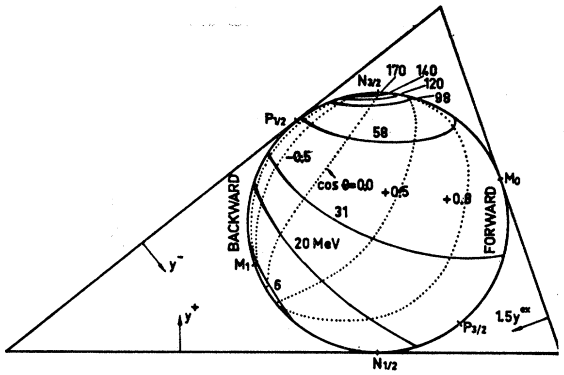

FIG. 1. The curves for the differential cross sections, summed over polarizations, $(|f|^2+|g|^2)$, obtained from the phase-shift analysis of Roper *et al.* (0 to 200 MeV).

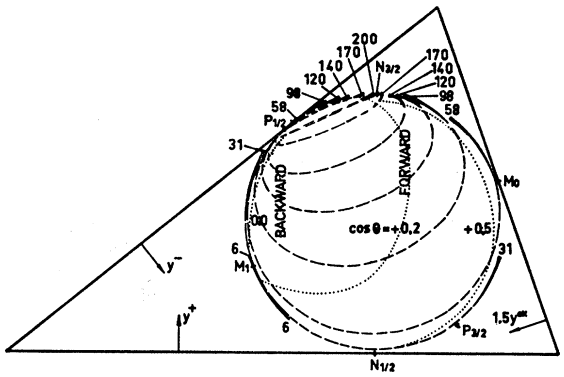

FIG. 3. The curves for the direct $(|f|^2)$ process (Roper *et al.*) (0 to 200 MeV).

amplitudes are either equal or opposite. This follows from the reality of the Clebsch-Gordan coefficients. Thus, if such a process dominates, the branching ratios will lie on the boundary curve. The points $N_{1/2}$ and $N_{3/2}$ marked in the diagrams, are obtained from the simple special cases where the scattering is dominated by a process with definite isospin in the direct channel (i.e., $A_{1/2}$ or $A_{3/2}$ dominates). Similarly the points P_T and M_T are obtained from a baryon and meson exchange process (with definite exchanged isospin T), respectively.

For a general and detailed description of the diagram see Ref. 2.

III. THE CURVES OBTAINED FROM EXPERIMENTAL DATA

There exists a large body of experimental data for the $\pi N \to \pi N$ differential cross sections. Furthermore, polarization measurements have been done at several energies. The data we have put in the diagrams fall into three categories:

(1) Phase-shift analysis up to 700 MeV (primarily that of Roper *et al.*);

(2) the dispersion-relation calculation by Höhler *et al.* for the forward scattering;

(3) direct measurements of $d\sigma^{(i)}/d\Omega$ fitted to a cosine or Legendre polynomial expansion (300–1500 MeV).

A computer program was prepared for the calculations and the plottings.

A. Phase-Shift Analysis

The data given in the form of an energy-dependent phase-shift analysis[5] are well suited to our purpose. The phase-shift analysis contains only a few physical assumptions (including CI). Even if the underlying principles are not exactly correct, this is a good way to parametrize the existing data and to interpolate between different experiments.

We have for the differential cross section

$$\frac{d\sigma^{(i)}}{d\Omega}=|f^{(i)}|^2+|g^{(i)}|^2, \tag{6}$$

where $f^{(i)}$ and $g^{(i)}$ are the direct and spin-flip amplitude, respectively. They are given by

$$f^{(i)}=(1/k)\sum_{l,T}\alpha_{iT}[(l+1)a_{l+}{}^T+la_{l-}{}^T]P_l(\cos\theta), \tag{7}$$

$$g^{(i)}=(1/k)\sum_{l,T}\alpha_{iT}[a_{l+}{}^T-a_{l-}{}^T]P_l{}^1(\cos\theta), \tag{8}$$

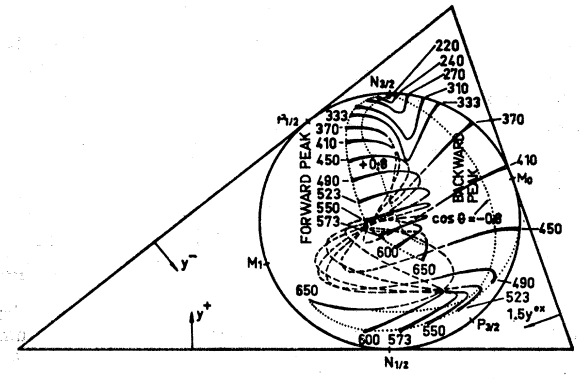

FIG. 2. As in Fig. 1 but for higher energies (200 to 650 MeV).

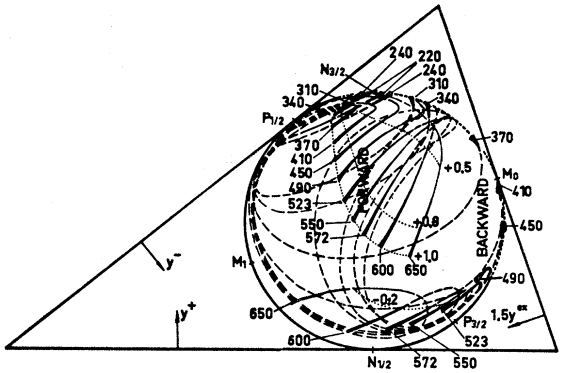

FIG. 4. As in Fig. 2 but for higher energies (200 to 650 MeV).

[5] L. D. Roper, R. M. Wright, and B. T. Feld, Phys. Rev. 138, B190 (1965).

where α_{iT} have the following values:

T \ i	+	−	ex
$\frac{1}{2}$	0	$\frac{2}{3}$	$-\sqrt{2}/3$
$\frac{3}{2}$	1	$\frac{1}{3}$	$\sqrt{2}/3$

and

$$a_{l\pm}{}^{T}=[\eta_{l\pm}{}^{T}\exp(2i\delta_{l\pm}{}^{T})-1]/2i. \quad (9)$$

The plots were drawn for the differential cross sections (6), and for the direct ($|f|^2$) and the spin-flip ($|g|^2$) process separately. The results are shown in Figs. 1–5, where the phase-shift analysis of Roper *et al.*[5] has been used. Every curve corresponds to a constant pion laboratory energy while the scattering angle θ is varied. Points with the same $\cos\theta$ are connected by a dotted line. When the sum of the cross sections is very small (less than 10% of the peak value) the curves are dashed; when this sum is large, the curves are drawn with a thicker line. Since the errors are roughly proportional to this sum, the curves are more reliable in the regions where they are thicker, i.e., usually in the forward and backward directions.

In Figs. 1 and 2 the curves are drawn for the sum of the direct and the spin-flip process. At very small energies the curves are close to the point M_1 ($T=1$ meson exchange), and around 200 MeV they are close to the point $N_{3/2}$ ($T=\frac{3}{2}$ dominates), as should be expected.

But we also make the interesting observation that the curves are *on the circle* both in the forward and the backward direction ($\cos\theta=\pm1$) for a wide energy region. In the forward direction this is true up to 200 MeV and in the backward direction up to at least 450 MeV,[6] where the phase-shift analysis becomes less reliable. We shall return to this observation several times below.

Figures 3 and 4 show the curves for the direct process $|f|^2$ and Fig. 5, the curves for the spin-flip process $|g|^2$. We can interpret a point in Fig. 1 or 2 as the average of the points for $|f|^2$ and $|g|^2$ separately at the same energy and $\cos\theta$. We see from these curves that the observation made above for $|f|^2+|g|^2$ at $\cos\theta=\pm1$ holds for much larger intervals of $\cos\theta$ for $|f|^2$, i.e., the curves move *along the circle* at $\cos\theta\simeq\pm1$. At low energies (below 200 MeV) $|g|^2$ contains primarily P waves (no S wave can contribute). Therefore $|g|^2$ has the same angular dependence ($\alpha\cos^2\theta$) in all three charge channels, and the curves reduce to points in the diagram. These points are close to the point $N_{3/2}$, as expected, and *on the circle*. The curves for $|f|^2$ deviate from the circle below 200 MeV only at values of $\cos\theta$ where the cross sections are very small. Thus, at 120 MeV, in the $\cos\theta$ interval where the deviation from the circle is greater than 1% of the diameter, the cross section

$$\int_{\text{interval}}\frac{d}{d\cos\theta}(|f^{(+)}|^2+|f^{(-)}|^2+|f^{(\text{ex})}|^2)d(\cos\theta)$$

is less than 4% of the total non-spin-flip cross section. In Figs. 6 and 7 the deviation from the circle in percent of the diameter is shown for $\cos\theta=+1$, $+0.6$, -0.6, and -1. On the other hand, the experimental cross sections have errors between 3 and 10%. This corresponds to an uncertainty of a point in the diagram of about 5 to 15% of the diameter. Comparing this to the small deviations found above, we conclude that the data are consistent with a hypothesis that the inequality (4) reduces to an equality in the energy region below the thresold of inelastic processes. We believe that if one adds very small phase shifts for the high angular momentum states one could fit the data with a phase-shift analysis in which the constraint is imposed that (4) is satisfied with the equality sign.

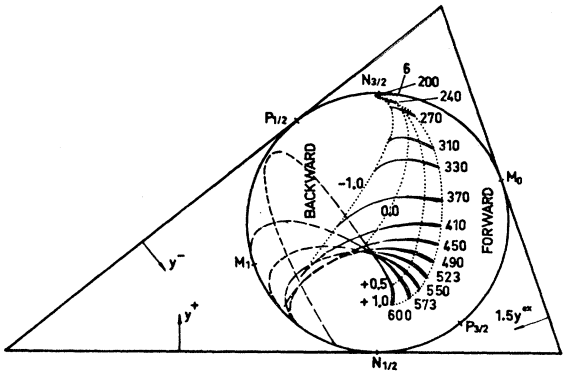

FIG. 5. The diagram for the spin-flip process ($|g|^2$) (Roper *et al.*) (0–600 MeV).

Another observation of interest is that the forward and backward peaks are well separated in the diagram, and that the curves for $|f|^2$ often tend to reduce to a point for values of $\cos\theta$ close to $+1$ or -1, while for $\cos\theta\approx0$, where the cross sections are small, the curves show a strong, almost discontinuous angular dependence. This tendency towards constant branching ratios

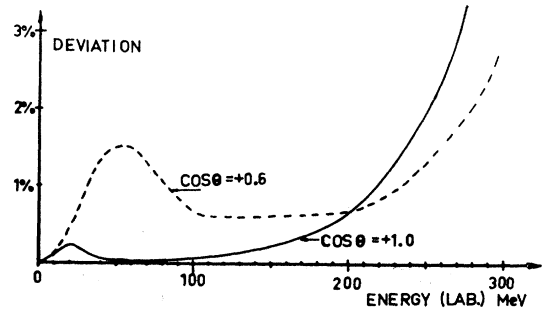

FIG. 6. Deviation from the circle in percent of the diameter in the forward direction (Roper *et al.*).

[6] A preliminary analysis using the phase-shift, analysis of A. Donnachie [CERN Report No. TH-690 (unpublished)] shows that in the backward direction the curves are on the circle up to 600 MeV. Above 600 up to 900 MeV the backward cross sections are very small and the accuracy of the experiments and the phase-shift analysis is much smaller.

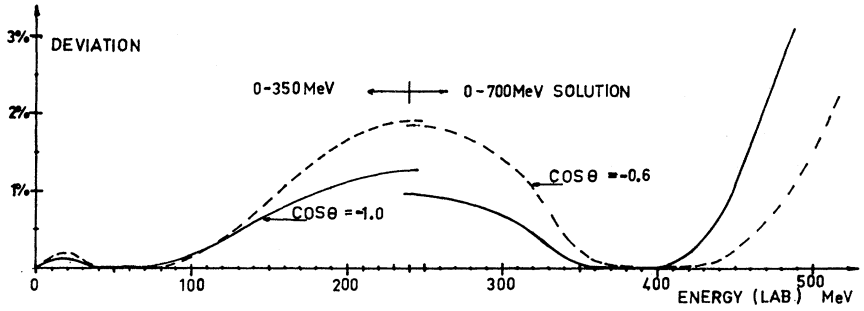

FIG. 7. Deviation from the circle in percent of the diameter in the backward direction (cf. Fig. 14).

is particularly evident when the curves are close to the boundary circle (see Figs. 3 and 4).

In Figs. 8–14 the curves for $|f|^2$ are shown when $\cos\theta$ is fixed and the energy is varied. These curves show clearly that the boundary circle is favored by the data. Between $\cos\theta=+0.4$ and 0.0, where the cross sections are extremely small, there is a sudden jump from an anticlockwise to a clockwise behavior.

B. The Dispersion Relation Calculation by Höhler et al.

Höhler *et al.*[7] have calculated the forward amplitudes using the optical theorem for the imaginary part and a dispersion relation for the real part. Thus the data put in are the total π^+p and π^-p cross sections, while the physical assumptions are the optical theorem, analyticity, and CI. Putting their results into the diagram we obtain the curves shown in Fig. 15. Here the scattering angle is constant ($\cos\theta=+1$) while the energy is varied from 0 to 30 GeV. We see that this curve shows the same results as obtained above from phase-shift analysis: To a high degree of accuracy it follows the circle below 200 MeV. This is thus an independent check of the observation.

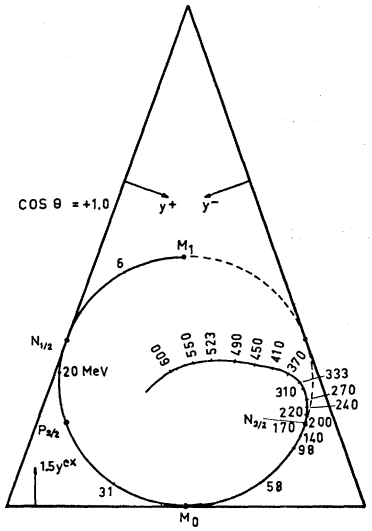

FIG. 8. The curve for forward scattering and variable energy (Roper *et al.*).

[7] G. Höhler, G. Ebel, and J. Giesecke, Z. Physik **180**, 430 (1964).

The curve shows an interesting spiraling behavior in which the "turning points" can be associated with resonances. At slightly below 200 MeV the curve passes the point $N_{3/2}$ where the scattering is dominated by the $\Delta(1236)$ resonance. Around 800 MeV there is a complicated structure, due to several $T=\frac{1}{2}$ resonances and one $T=\frac{3}{2}$ resonance[8]: $N(1525)$, $N(1570)$, $N(1670)$, $N(1688)$, $N(1700)$, and $\Delta(1670)$. The next resonances, $\Delta(1920)$ at 1.35 GeV, $N(2190)$ at 1.94 GeV, $\Delta(2420)$ at 2.51 GeV, and $N(2650)$ at 3.12 GeV, coincide with the turning points of the curve. Furthermore, the $T=\frac{1}{2}$ resonances are to the left while the $T=\frac{3}{2}$ resonances are to the right.

If we compare Fig. 15 with the corresponding curve for backward scattering (obtained from phase-shift analysis), Fig. 14, we see that both show a similar spiraling behavior, although in opposite directions.

C. Direct Measurements of $d\sigma^{(i)}/d\cos\theta$

The experimental data[9–14] are given as coefficients in a cosine or Legendre polynomial expansion

$$\frac{d\sigma^{(i)}}{d(\cos\theta)}=\sum_n a_n\cos^n\theta \quad \text{or} \quad \frac{d\sigma^{(i)}}{d(\cos\theta)}=\sum_n b_n P_n(\cos\theta). \quad (10)$$

When the experiments had been done at slightly different energies in the different charge channels, we used linear interpolation between different experiments in order to get comparable cross sections. The curves covering the energy region 300–1500 MeV are shown in Figs. 16 to 19. The curves below 700 MeV and those obtained from the phase-shift analysis show a similar behavior.

[8] A. H. Rosenfeld, A. Barbaro-Galtieri, W. J. Podolsky, L. R. Price, Matts Roos, Paul Soding, W. J. Willis, and C. G. Wohl, Rev. Mod. Phys. **39**, 1 (1967).

[9] D. L. Lind, B. C. Barish, R. J. Kurz, P. M. Ogden, and V. Perez-Mendez, Phys. Rev. **138**, B1509 (1965).

[10] P. M. Ogden, D. E. Hagge, J. A. Helland, M. Banner, J.-F. Detoeuf, and J. Teiger, Phys. Rev. **137**, B115 (1965).

[11] J. A. Helland, C. D. Wood, T. J. Devlin, D. E. Hagge, M. J. Longo, B. J. Moyer, and V. Perez-Mendez, Phys. Rev. **134**, B1097 (1964).

[12] J. A. Helland, T. J. Devlin, D. E. Hagge, M. J. Longo, B. J. Moyer, and C. D. Wood, Phys. Rev. **134**, B1064 (1964).

[13] L. Guerriero, Proc. Roy. Soc. (London) **A289**, 470 (1966).

[14] P. J. Duke, D. P. Jones, M. A. R. Kemp, P. G. Murphy, J. D. Prentice, and J. J. Thresher, Phys. Rev. **149**, 1077 (1966). I am grateful to Dr. D. P. Jones for providing me with the original data.

At higher energies the backward and forward peaks are still well separated in the diagram, and in the backward direction the curves are close to the boundary curve. In fact, at energies around 500 MeV and around 1.3 GeV the curves are slightly outside the physical region, which is in contradiction to CI. However, the experimental errors are of the same order of magnitude as the deviation. Around 550 MeV the largest deviation is 8% of the diameter of the circle. On the other hand the experimental errors in the cross sections correspond to an uncertainty of a point in the diagram of about 6% in the direction of the radius of the circle. Around 1.3 GeV the deviation is at most 6% while the errors are around 7%. Furthermore, if one looks at the measured cross sections and not at the values obtained from the fit to Eq. (10), the deviations are smaller. This comparatively large difference between the fitted and measured cross sections can be understood from the fact that in the backward direction the expansion (10) is a sum of large terms with alternating signs. We therefore conclude that the measured cross sections are up to 1.5 GeV consistent with the inequality (4).

In the forward direction at energies above 1 GeV, where the cross sections show a diffraction peak behavior, the curves (Figs. 18 and 19) tend to reduce to a point close to M_0.

IV. A POSSIBLE EXPLANATION

The results which were obtained above can be considered as experimental facts. The most important observation was that the triangle inequalities, which are equivalent to Eq. (4), reduce to an equality in the elastic region and in backward scattering. In terms of the isospin amplitudes this means that these are parallel or antiparallel in the complex plane.

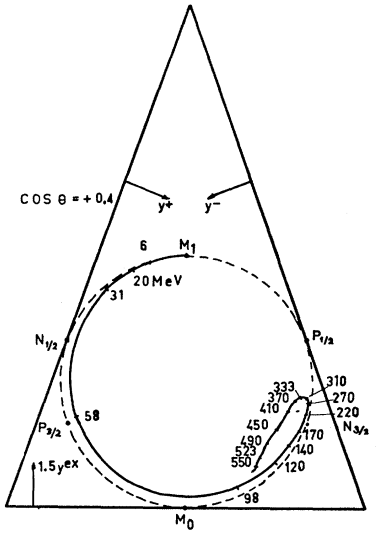

FIG. 10. The curve for $|f|^2$ with $\cos\theta = +0.4$ and variable energy (Roper *et al.*).

One would of course expect to have a simple explanation of a fundamental nature to a problem which is expressible in such simple terms. However, we have not succeeded in obtaining this result from the well-known principles by a simple argument. The isospin amplitudes are generally considered to be independent, while our analysis shows that they are coupled so that they have the same or opposite phase.

Below we suggest one possible way of modifying the formalism. We find it appealing because of its simplicity.

Looking at the diagrams, especially Figs. 8 to 15, one sees a certain graphical resemblance to the Argand diagram for a partial-wave amplitude $(\eta_j e^{2i\delta_j i} - 1)/2i$. In the latter, probability conservation or unitarity requires

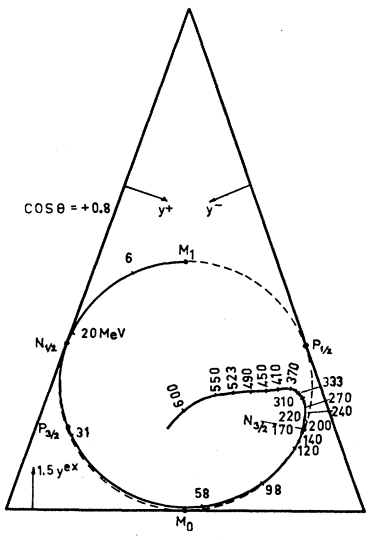

FIG. 9. The curve for $|f|^2$ with $\cos\theta = +0.8$ and variable energy (Roper *et al.*).

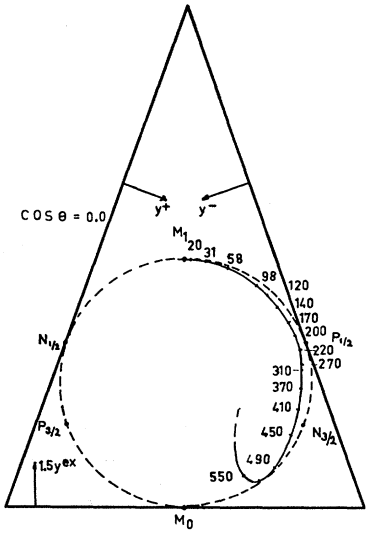

FIG. 11. The curve for $|f|^2$ with $\cos\theta = 0.0$ and variable energy (Roper *et al.*).

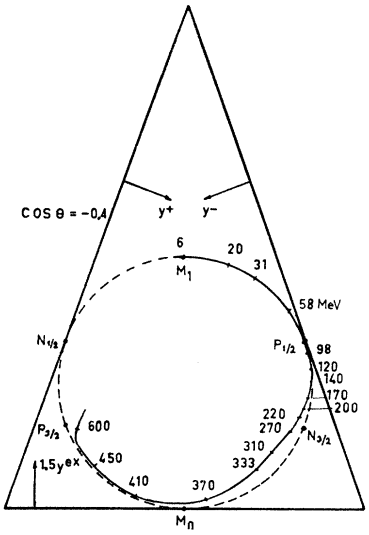

FIG. 12. The curve for $|f|^2$ with $\cos\theta=-0.4$ and variable energy (Roper *et al.*).

that $\eta_j=1$ in the elastic region. Graphically this means that the amplitude follows a circular path in the diagram. When inelastic channels are open, we have $\eta_j<1$ and points inside the circle are allowed. This would suggest that the observed effect might be interpreted as due to a unitarity condition in charge space.

In the usual formalism it is difficult to define for the isospin amplitudes a concept similar to probability conservation for the amplitudes of definite angular momentum. We also note that isospin is *not* conserved under crossing. When the S matrix, which is diagonalized in the isospin in the s channel, is transformed by the crossing matrices (see below), it will contain off-diagonal elements in the u and t channels. Considering only the isospin part of the interaction, we define below an S matrix which remains diagonal under crossing.

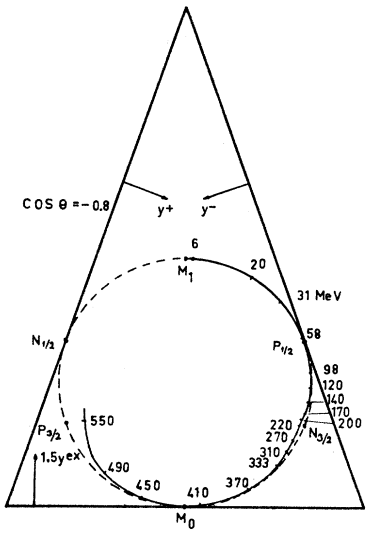

FIG. 13. The curve for $|f|^2$ with $\cos\theta=-0.8$ and variable energy (Roper *et al.*).

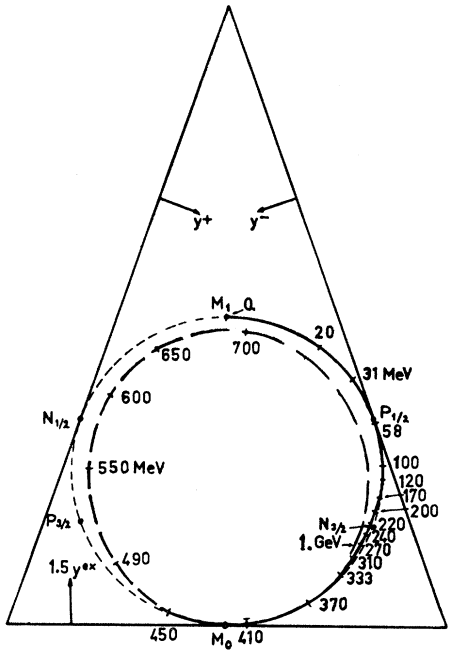

FIG. 14. The curve obtained for backward scattering energy (Roper *et al.*). See also Ref. 6.

Let us look at the following linear combinations of the isospin amplitudes, which as we shall see have simple transformation properties under crossing and in terms of which the condition to be on the boundary circle takes a simple form [cf. Eq. (5) and Eq. (19) below]:

$$\sqrt{2}D_{\pm}=A_{1/2}\pm i\sqrt{2}A_{3/2}, \tag{11a}$$

$$\sqrt{2}D_{\pm}{}^{u}=A_{1/2}{}^{u}\pm i\sqrt{2}A_{3/2}{}^{u}, \tag{11b}$$

$$\sqrt{2}D_{\pm}{}^{t}=(\sqrt{\tfrac{1}{2}})A_{0}{}^{t}\pm(i\sqrt{\tfrac{3}{2}})A_{1}{}^{t}, \tag{11c}$$

where $A_{1/2}$ and $A_{3/2}$ are the (direct) isospin amplitudes in the s channel, and $A_T{}^u$ and $A_T{}^t$ are the isospin amplitudes in the u and t channels. We can also consider $A_T{}^u$ and $A_T{}^t$ as amplitudes of definite exchanged isospin in the s channel. These are related to A_T by crossing matrices

$$\begin{pmatrix}A_{1/2}{}^{u}\\ A_{3/2}{}^{u}\end{pmatrix}=\begin{pmatrix}-\frac{1}{3} & \frac{4}{3}\\ \frac{2}{3} & \frac{1}{3}\end{pmatrix}\begin{pmatrix}A_{1/2}\\ A_{3/2}\end{pmatrix}, \tag{12a}$$

$$\begin{pmatrix}A_{0}{}^{t}\\ A_{1}{}^{t}\end{pmatrix}=\begin{pmatrix}\frac{1}{3}\sqrt{6} & \frac{2}{3}\sqrt{6}\\ -\frac{2}{3} & \frac{2}{3}\end{pmatrix}\begin{pmatrix}A_{1/2}\\ A_{3/2}\end{pmatrix}. \tag{12b}$$

For the amplitudes D above, these simply become diagonal matrices with phase factors as elements:

$$D_{\pm}=e^{\pm i\varphi u}D_{\mp}{}^{u}=e^{\pm i\varphi t}D_{\pm}{}^{t}, \tag{13}$$

where $\cos\varphi^u=\frac{1}{3}$, and $\cos\varphi^t=\sqrt{\frac{1}{3}}$. Similarly, if we denote the initial isospin states as $|\pi N,T\rangle$, $|\pi\bar{N},T\rangle$, $|\pi\pi,T\rangle$ in

the s, u, and t channels, respectively, the states

$$\sqrt{2}|\pi N,\pm\rangle = |\pi N,\tfrac{1}{2}\rangle \pm i\sqrt{\tfrac{1}{2}}|\pi N,\tfrac{3}{2}\rangle, \quad (14a)$$

$$\sqrt{2}|\pi \bar{N},\pm\rangle = |\pi \bar{N},\tfrac{1}{2}\rangle \pm i\sqrt{\tfrac{1}{2}}|\pi \bar{N},\tfrac{3}{2}\rangle, \quad (14b)$$

$$\sqrt{2}|\pi\pi,\pm\rangle = \sqrt{2}|\pi\pi,0\rangle \pm i\sqrt{\tfrac{2}{3}}|\pi\pi,1\rangle, \quad (14c)$$

differ from each other only by a phase factor and are thus "crossing independent."

We now define a matrix

$$S=\frac{1}{\sqrt{\sigma}}\begin{pmatrix} D_+ & 0 \\ 0 & D_- \end{pmatrix}, \quad (15)$$

where

$$\sigma=\tfrac{1}{2}(|D_+|^2+|D_-|^2)=\tfrac{1}{2}(|A_{1/2}|^2+2|A_{3/2}|^2) \propto \sigma^{(+)}+\sigma^{(-)}+\sigma^{(\mathrm{ex})}.$$

Then

$$S\begin{pmatrix} |\pi N,-\rangle \\ |\pi N,+\rangle \end{pmatrix}=\frac{1}{\sqrt{\sigma}}\begin{pmatrix} D_+|\pi N,-\rangle \\ D_-|\pi N,+\rangle \end{pmatrix}$$

can be considered as one way of representing the final state, since using Eq. (11) we get

$$D_+|\pi N,-\rangle+D_-|\pi N,+\rangle = A_{1/2}|\pi N,\tfrac{1}{2}\rangle+A_{3/2}|\pi N,\tfrac{3}{2}\rangle. \quad (16)$$

This representation has the symmetric property that under crossing the matrix S transforms into other *diagonal* matrices S^u and S^t:

$$S^u=\frac{1}{\sqrt{\sigma}}\begin{pmatrix} D_+^u & 0 \\ 0 & D_-^u \end{pmatrix}, \quad (17a)$$

$$S^t=\frac{1}{\sqrt{\sigma}}\begin{pmatrix} D_+^t & 0 \\ 0 & D_-^t \end{pmatrix}. \quad (17b)$$

We can represent the final state simultaneously in any of the forms

$$S\begin{pmatrix} |\pi N,-\rangle \\ |\pi N,+\rangle \end{pmatrix}=S^u\begin{pmatrix} |\pi \bar{N},-\rangle \\ |\pi \bar{N},+\rangle \end{pmatrix}=S^t\begin{pmatrix} |\pi\pi,-\rangle \\ |\pi\pi,+\rangle \end{pmatrix}. \quad (18)$$

The advantage of working with linear combinations of the type (11) is more apparent in a reaction $K^+p \to KN\pi$ (which from the point of view of isospin is equivalent to $\pi \to N\bar{N}\pi$). We considered this reaction in detail in Ref. 1. There we denoted the final states with definite intermediate isospin in the $N\pi$ system by $|N_{1/2}\rangle$ and $|N_{3/2}\rangle$, and the corresponding amplitudes by $a_{1/2}$ and $a_{3/2}$. On the other hand, for final states with definite isospin T in the $K\pi$ and KN systems we used the notations $|K_T\rangle$, b_T and $|Y_T\rangle$, c_T, respectively. Since

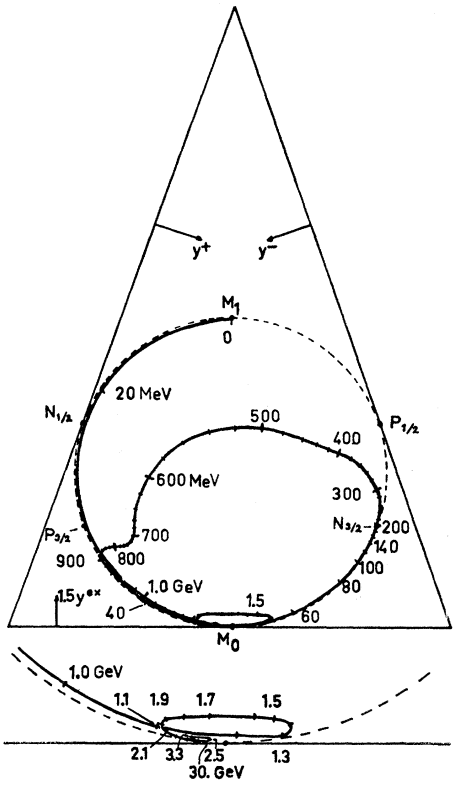

FIG. 15. The curve obtained from the dispersion relation calculation of Höhler *et al.* for forward scattering with variable energy.

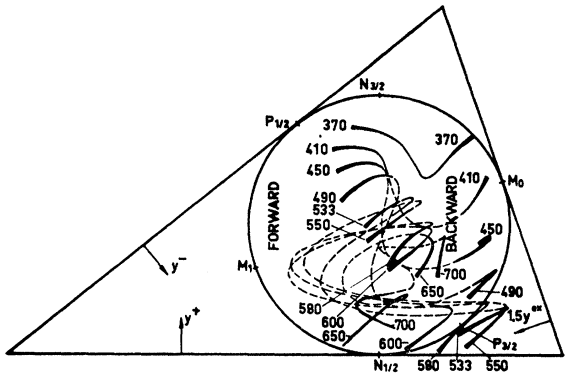

FIG. 16. The curves obtained from data on direct measurements of the differential cross sections (370–700 MeV).

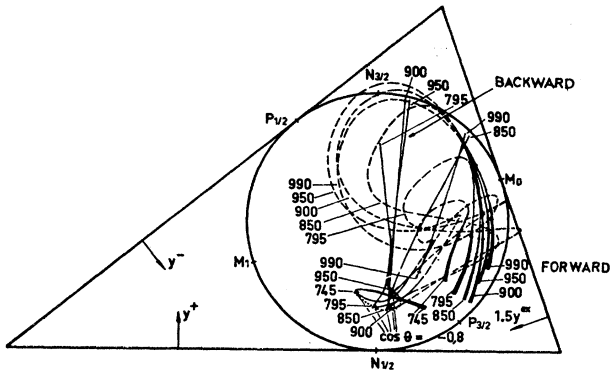

FIG. 17. The curves obtained from data on direct measurements of differential cross sections (700–1000 MeV).

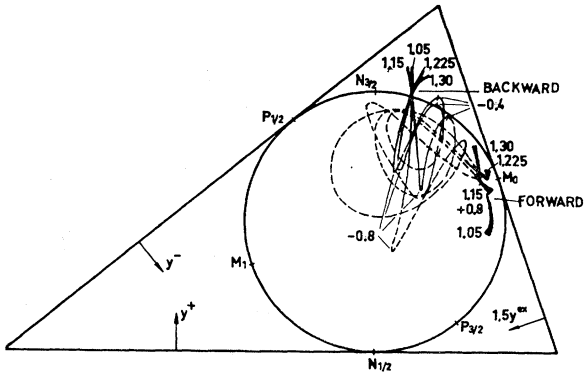

FIG. 18. The curves obtained from data on direct measurements of the differential cross sections (1.0–1.45 GeV).

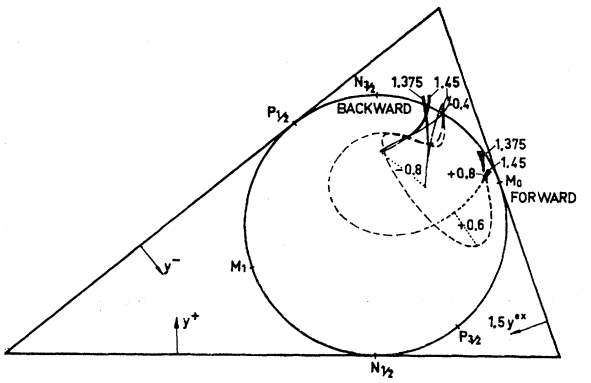

FIG. 19. The curves obtained from data on direct measurements of the differential cross sections (1.0–1.45 GeV).

intermediate isospin is *not* a conserved quantity the 2×2 S matrix for the isospin part of the interaction is not diagonal. But if we impose the symmetry that the S matrix should be diagonal in all three ways of coupling the isospins of the three final particles, one can do it using the linear combinations $a_{1/2}\pm ia_{3/2}$, $b_{1/2}\pm ib_{3/2}$, or $c_0\pm ic_1$, as diagonal elements. Similarly the states $|K_{1/2}\rangle\pm i|K_{3/2}\rangle$, $|N_{1/2}\rangle\pm i|N_{3/2}\rangle$, and $|Y_0\rangle \pm i|Y_1\rangle$ differ from each other only by a phase factor and are thus independent of recoupling of the isospins.

Let us now turn to $\pi N\rightarrow\pi N$ and the experimental observation. In terms of the amplitudes $D_\pm$, the condition that the two isospin amplitudes have the same or opposite phase is simply that $D_\pm/\sqrt{\sigma}$ be equal to a phase factor

$$D_\pm/\sqrt{\sigma}=e^{i\delta_\pm}. \tag{19}$$

But this is just the condition of unitarity for the matrix S

$$SS^\dagger=1. \tag{20}$$

Furthermore, the matrices S^t and S^u are then also unitary; thus this unitarity is "crossing independent."

This model is at least qualitatively able to explain why the curves deviate from the circle at energies above the inelastic thresholds. Then, because of the possible many-particle final states, we have to introduce an absorption coefficient in Eq. (19). The question why at higher energies the curves follow the circle in the backward direction remains open. Maybe one can find arguments for thresholds in momentum transfer since the elastic process has a smaller t in the backward direction ($t=-4p_{\text{c.m.}}^2$) than in any inelastic process.

V. CONCLUDING REMARKS

The most important result obtained here is that the inequality (4) is in fact satisfied as an equality below the threshold for inelastic processes and in the backward direction up to at least 450 MeV.[6] We wish to emphasize that this condition puts very strong constraints on the $\pi N\rightarrow\pi N$ cross sections. In terms of phase-shift analysis such a condition gives a large number of relations between the phases. Already if we impose this constraint only in forward and backward scattering, we obtain two conditions on the phases which at low energies are very few in number. We suggest that those who do phase-shift analyses try to include constraints of this type. It would also be interesting to have high-accuracy experiments on all three charge channels in the low-energy region and in the backward direction at intermediate energies (200–1000 MeV).

The difficulty in explaining the observation with the present formalism suggests that the formalism may have to be modified. In Sec. IV we suggested one way in which this could be done. We find this model appealing because of its simplicity and because it puts on an equal footing the different ways of coupling the particles to states of definite isospin.

ACKNOWLEDGMENTS

The author is indebted to Dr. A. Donnachie and Dr. C. Lovelace, CERN, Dr. B. Lautrup, Nordita, Professor P. Jauho, and Professor P. Tarjanne, Helsinki, and Professor G. Ekspong, Stockholm, for helpful discussions. He also wishes to thank Professor K. V. Laurikainen, who in many ways helped in the completion of this work and Dr. P. O. Lipas, who kindly checked the English.